The supersonic flow past a leading edge separation bubble

By A. W. SHARP
Department of the Mechanics of Fluids, University of Manchester

(Received 24 August 1958)

The supersonic flow field outside a leading edge separation bubble has been computed in detail by a special application of the method of characteristics. Experimental observations on a two-dimensional square-nosed flat plate at $M = 1{\cdot}96$ formed the initial data, and base points were established on the plate surface. Computations proceeded outwards and upstream to the sonic line and bow wave, the bow wave entropy gradient being taken into account. The shape of the sonic line was found to be very sensitive to the conditions along the plate surface. Streamlines and iso-Mach lines have been interpolated and are presented. Good agreement was found at the intersection of the network and the bow wave between computed values and those given directly by the shock wave equations. A comparison has been made with interferometric results from France.

1. Introduction

The two-dimensional supersonic flow past a square-nosed flat plate involves a detached bow shock wave with a resulting region of mixed flow. Also, the boundary layer on the front face of the plate is unable to negotiate the right-angle corner and separates, reattaching to the plate some distance downstream. The region enclosed between the separated boundary layer, or mixing region, and the solid boundary is termed a separation bubble. Such bubbles have been noted previously, for instance by Holder & Chinneck (1954), who photographed and pressure-plotted the region at Mach numbers below that of the present work. Separation bubbles have also been observed to occur on the leading edge of thin aerofoils.

After traversing the bow shock wave, the flow close to the centre line is subsonic, but accelerates to supersonic speed, attaining a Mach number of unity at the sonic line which joins the bow wave sonic point to the sonic point on the plate. Of these two end-points, the former is easily determined from the bow wave slope, and the latter is generally accepted to lie at the corner of the plate. However, the shape of the sonic line between them and the interdependence between its shape and the conditions along the separated region and the solid boundary farther downstream are not known.

It appeared possible that the supersonic portion of the external flow field might be computed by the method of characteristics if the flow conditions along the plate were known. It was hoped that the shape and location of the sonic line might be determined, and that its relationship with the boundary conditions

would be clarified. The procedure followed is described in the present paper, the basic data being the experimentally determined pressure distribution and bubble profile. On suitably spaced base points a characteristics network has been constructed, which extends upstream to the inboard portion of the sonic line, and outwards to the bow wave. In this way, it has proved possible to determine the inboard part of the sonic line, and also the streamlines and iso-Mach lines in the supersonic region.

In § 2 below the basic experimental results are described, whilst their conversion to usable form is discussed in § 3. Details of the actual computation follow in § 4 and a discussion of the resultant flow field is given in § 5.

2. The basic experimental data

The flat plate of $\frac{9}{32}$ in. thickness was mounted at zero incidence in an intermittent vacuum-operated wind tunnel of working section dimensions 5 in. × 4 in.; this wind tunnel has been described previously by Bardsley & Mair (1951). The plate spanned the entire 4 in. width of the working section and was supported

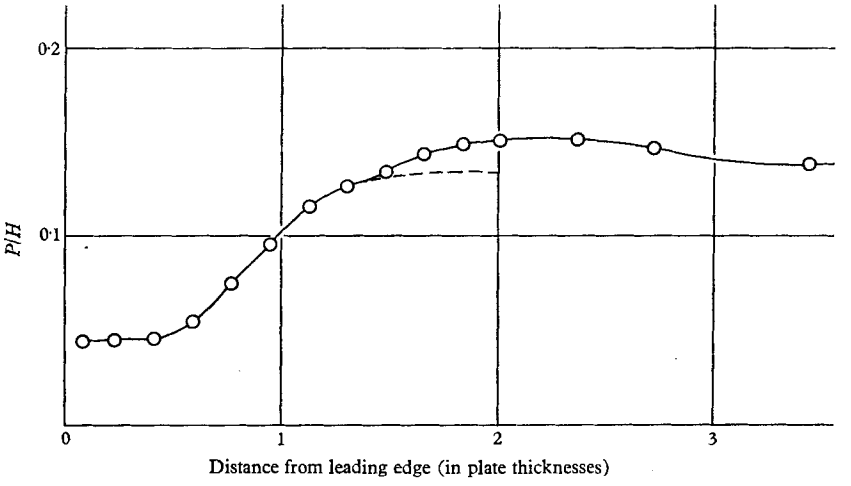

FIGURE 1. Static pressure distribution near leading edge of flat plate.

from downstream by two arms. The Mach number was 1·96, and atmospheric stagnation conditions yielded a free stream Reynolds number of $3{\cdot}44 \times 10^5$ with a length scale of one inch. The humidity of the air was maintained well below 0·2 g/kg in order to avoid condensation effects. Pressure tappings of 0·015 in. diameter in the surface of the plate communicated, via a buried tube, with an absolute mercury manometer of accuracy ± 0·1 mm of mercury.

The measured pressure distribution on the plate is shown in figure 1. P is the static pressure and H the free stream stagnation pressure. The broken curve at the downstream end indicates the expected return to free stream static pressure. The upward kink in the observed curve is thought to be due to compression and rarefaction disturbances propagated downstream from the bow wave-boundary layer interaction on the tunnel window, and has been ignored in what follows. As

would be expected, the pressure inside the front portion of the bubble is constant, but is followed by a rapid pressure rise through the recompression fan.

The flow pattern was photographed, using a conventional two-mirror schlieren system with a flash-tube as light source. A photograph of the nose region is shown in figure 2 (plate 1). The apparent thickness of the shock waves and separated boundary layer is due to interaction with the window boundary layer, and to the flow not being truly two-dimensional.

3. Conversion of data

The static pressure distribution was first converted into the surface Mach number distribution, allowance being made for the loss of stagnation pressure suffered when the stagnation streamline traversed the normal bow wave. The pressure across the separated region was assumed to be constant at each station. The schlieren photograph was then enlarged to eight times natural size, and the ordinates of the bubble profile were carefully measured at a number of stations. Similar measurements were taken of the bow wave location and shape. It was now necessary to fit analytic curves to these profiles in order that the ordinates and slopes could be calculated at all points.

The bow wave co-ordinates were fitted very well by a cubic over the range required. From this curve, the slope of the bow wave at any ordinate could be calculated, so that the bow wave sonic point was located precisely. The fitting of curves to the bubble profile proved to be rather more difficult. The initial direction of the separated layer was calculated, assuming sonic conditions at the corner, and knowing the bubble static pressure. The photographic ordinates were well fitted by a combination of three curves, namely an ellipse from the leading edge to just beyond the point of maximum height, followed by a straight line down towards the surface, and a circular arc between the line and the surface. Of these curves, the ellipse had the correct slope at the leading edge, the straight line was tangential to both the ellipse and the circular arc, and the plate surface was tangential to the arc. A trial set of computations based on this boundary, however, produced kinks in the iso-Mach lines and flaws in the recompression shock wave. These flaws were traced back to the concave portion of the profile, and it was realized that a smooth distribution of $(\theta+t)$ along the boundary had not been obtained, although both θ, the flow direction, and t, a function of Mach number, individually had smooth distributions. This requirement for a smooth $(\theta+t)$ distribution proved difficult to satisfy, but was eventually achieved by fitting a parabola and a quintic to the recompression region. The condition that $(\theta+t)$ must vary smoothly along the boundary therefore severely limited the choice of curves available for fitting, and also demonstrated the close relationship between surface conditions and sonic line shape.

4. Details of the computations

4.1. *The first approximation*

The information available, namely the distributions of flow direction, Mach number, and bubble height along the surface made it possible to commence the calculations after selecting suitably spaced base points. These were selected to

coincide with the static holes over most of the bubble region, but this spacing was varied where necessary. Thus, close to the leading edge the bubble curvature is much increased, and the base points are accordingly much closer together; conversely, far downstream conditions become almost constant, and a much wider spacing is acceptable. The data were sufficient to permit the computation, by the method of characteristics, of the flow field enclosed by the first minus Mach line from the leading corner and the plus Mach line from any surface point downstream. (Plus and minus Mach lines are defined in figure 3.) Since the surface static pressure becomes constant downstream of the bubble, the flow field may be investigated as far downstream, and hence as far outwards as is required, the conditions on all plus Mach lines being known.

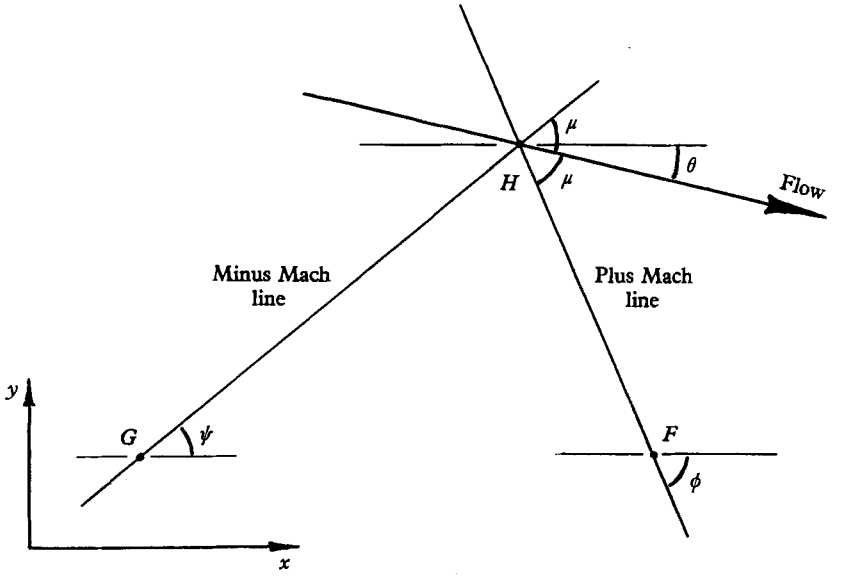

FIGURE 3. Angles used in computing H from F and G.

Using Cartesian co-ordinates x, y, the characteristic equations for the Mach lines may be written (see Meyer 1948),

$$\frac{dy}{dx} = \tan(\theta \mp \mu), \tag{1}$$

$$d\theta \mp \frac{\sin\mu\cos\mu}{\rho a^2}\,dp = 0, \tag{2}$$

where the upper and lower signs refer to plus and minus Mach lines respectively. (μ is the Mach angle, θ the angle between the x-axis and the velocity vector, ρ the density, a the velocity of sound, and p the pressure.) Equation (2) may be rewritten in the form

$$d(t \pm \theta) + d\sigma \sin 2\mu = 0,$$

where

$$dt = \frac{dq}{q}\cot\mu \quad \text{and} \quad d\sigma = \frac{ds}{2\gamma R}. \tag{3}$$

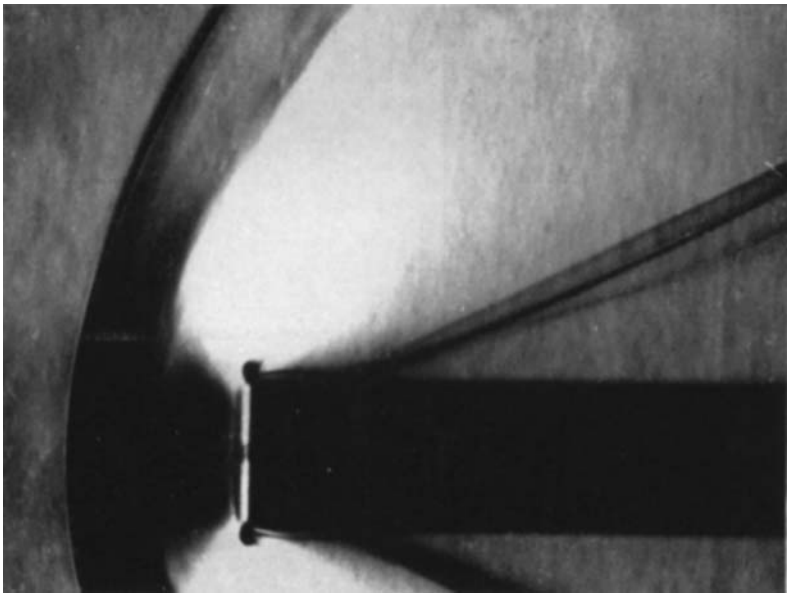

FIGURE 2 (plate 1). The separation bubble.

Here, q is the velocity magnitude, s the specific entropy, γ the ratio of specific heats, and R the gas constant. It may be shown that

$$t = \mu - \tfrac{1}{2}\pi + \lambda^{-1}\cot^{-1}(\lambda^{-1}\tan\mu), \tag{4}$$

where $$\lambda = [(\gamma-1)/(\gamma+1)]^{\frac{1}{2}}.$$

The function $(1000-t)$, normally referred to as the pressure number, has been tabulated for $\gamma = 1{\cdot}400$ by Herbert & Older (1946).

As a first approximation, the difference in entropy change between adjacent streamlines across the curved bow wave was neglected, so that equation (3) became

$$d(t \pm \theta) = 0. \tag{5}$$

From equations (1) and (5), a network of points was constructed by the usual method of characteristics, extending upstream and outwards and based on the surface points. In the expansion fan at the leading corner, minus Mach lines were chosen at intervals of 5° in θ. Iso-Mach lines were drawn in by interpolation for Mach numbers, M, equal to 1·1, 1·2, 1·3, and were found to be kinked, due to an irregular surface distribution of $(\theta+t)$. The mechanism of this effect may be explained as follows. In figure 4, ignoring entropy differences,

$$(\theta+t)_A = (\theta+t)_B.$$

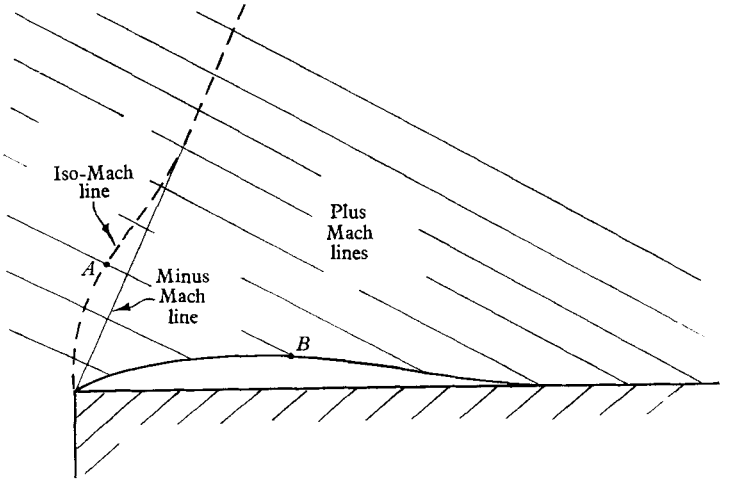

FIGURE 4. Shape of iso-Mach lines.

Along the iso-Mach line, by definition, M = constant, so that μ and t are also constant. Thus using suffixes M, B, to denote conditions on the iso-Mach line and boundary respectively, and since $(\theta+t)_M = (\theta+t)_B$, we have

$$\theta_M = (\theta+t)_B - t_M = (\theta+t)_B - \text{constant}.$$

Hence, once $(\theta+t)_B$ has settled down to its constant value, it follows that θ_M = constant. Moreover, we now have θ_M and t_M both constant so that $(\theta-t)_M$ = constant, i.e. the iso-Mach line is also a minus Mach line. Also, since μ_M, θ_M are constant along this line, $\psi_M = (\theta+\mu)_M$ = constant, and the iso-Mach lines and minus Mach lines are therefore straight in this region.

It can thus be seen that kinks in $(\theta + t)_B$ would give rise to corresponding kinks in the distribution of θ_M along the iso-Mach line, leading, in turn, to kinks in the line itself. The correctness of this diagnosis was demonstrated by the elimination of the iso-Mach line kinks when the $(\theta + t)_B$ distribution was smoothed out by the modified choice of boundary curves already discussed.

4.2. *The entropy correction*

The curvature of the bow shock wave causes an entropy gradient across the flow downstream, each streamline having an entropy value which is constant but different from those of its neighbours. Accordingly, in order to evaluate the second term in equation (3), it was necessary to identify the streamline upstream of the bow wave which corresponded to the point under computation. This was achieved by calculating the mass flow between the first approximation to the point and the boundary. Thus for H (figure 3), the mass flow across FH was calculated, where F was already corrected for entropy (and hence the mass flow between F and the boundary was known). Thus, the mass flow between the boundary and H was obtained, thereby locating the H-streamline upstream of the bow wave. From this ordinate, the corresponding bow wave slope was derived and hence the entropy increase. This in turn yielded the entropy differences $d\sigma$ between H and F, and between H and G, which were required for insertion in equation (3). The flow and position parameters for H were then recalculated with this entropy correction included. Fortunately, the correction was not large enough to necessitate any iterative repetition of the procedure. (No correction was applied for entropy changes produced by the recompression. This is not likely to lead to any appreciable error since, in the region computed, much of the recompression takes place through a fan or weak shock.) This system was used in computing the whole flow field, apart from the region very close to the sonic line which required special treatment as will be seen in § 4.3 below.

4.3. *The final step to the sonic line*

The usual system of characteristics computations as outlined in 4.1 above may be shown to assume that the Mach line segments are circular arcs. This assumption is fully justified in general for small steps, but in the neighbourhood of the sonic line the Mach lines curve strongly, and have been shown by Holt (1949) to behave like semi-cubical parabolae. This holds only for small $\nu = \frac{1}{2}\pi - \mu$, and was here taken to be true for $M \leqslant 1{\cdot}02$, corresponding to $\nu = 0{\cdot}2$ radian. Accordingly, a method was used whereby ϕ, ψ (figure 3) were averaged along a semicubical parabola rather than the usual circular arc. Thus if the semicubical parabola is $y^{*3} = cx^{*2}$, and the chord is $y^* = x^* \tan \eta$ (see figure 5), then it may be shown that $\tan \eta = \frac{3}{2} \tan \beta$. This has utilized an origin on the sonic line with the x-axis in the local flow direction. Translation of the origin to that of the characteristics network will not affect the purely angular relationship between η and β, but the angles to be averaged must be related to a new reference direction before the equation is used. This new reference direction, θ_s, will be the flow direction at the intersection of the sonic line and the relevant Mach line. Since the entropy term is negligible for this last step to the sonic line (see below), and since $t = 0$ on the sonic line, it

follows that θ_s is identical with the value of $\theta \pm t$ on the plus or minus Mach line. In place of the old ϕ, ψ (Mach line inclinations to free stream direction), we use ϕ^*, ψ^*, where for a plus Mach line, $\phi^* = \phi - \theta_{s+} = \theta - \mu - \theta_{s+} = -(\mu + t)$; and for a minus Mach line, $\psi^* = \psi - \theta_{s-} = \theta + \mu - \theta_{s-} = \mu + t$. Here, for any point, $\theta_{s+} = \theta + t$ (along the plus Mach line) and $\theta_{s-} = \theta - t$ (along the minus Mach line). Then, on a plus Mach line, $\eta = \phi^{*H}_F = \tan^{-1}(\frac{3}{2}\tan\phi^*)$ and, on a minus Mach line, $\eta = \psi^{*H}_G = \tan^{-1}(\frac{3}{2}\tan\psi^*)$, where the affices $\frac{H}{F}$, $\frac{H}{G}$ refer to average quantities between the points. Then $\phi^H_F = \phi^{*H}_F + \theta_{s+}$ and $\psi^H_G = \psi^{*H}_G + \theta_{s-}$. These latter values, ϕ^H_F, ψ^H_G (averages along the semicubical parabolae) were then used to determine x_H, y_H, as before.

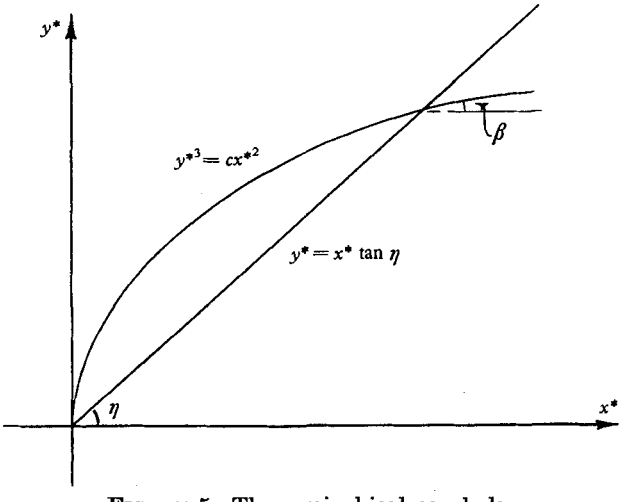

FIGURE 5. The semicubical parabola.

As will now be seen, it was not possible to correct this final step for entropy variations, but it will be shown that the correction would be negligible. The effect of the entropy correction is to increase the Mach number of the first approximation. Thus, in order to attain a specified Mach number M, it is necessary, when calculating the first approximation, to overshoot M to a lower value, which is then raised to the required value M by the correction. This is clearly impossible for $M = 1$, since the characteristics become imaginary for $M < 1$. However, this inability to correct for entropy is of no consequence, since the correction would be negligible for two reasons: (i) the step from $M = 1{\cdot}02$ to $M = 1{\cdot}00$ is geometrically very small, so that $d\sigma$ would be negligible; (ii) in this region, $\mu \to 90°$, hence $\sin 2\mu \to 0$. Accordingly, the correction term $d\sigma \sin 2\mu$ will be extremely small and its omission of no importance.

4.4. *Summary of the computations*

The use of the techniques described above, in §§ 4.1, 4.2 and 4.3, made possible the computation of almost all the supersonic flow field downstream of the sonic line and bow wave. Where necessary, due to rapid variation of the parameters, the mesh size was reduced in order to maintain the accuracy. The network was extended outwards until it intersected the bow wave.

Only about one-third of the sonic line proved to be calculable, since at C (see figure 6), about 0·85 plate thickness from the surface, the line curved strongly upstream. Outboard of this point, computations ceased to be possible upstream of the minus Mach line CA, leaving an indeterminate supersonic zone CAS, enclosed by the outermost portion of the sonic line, part of the bow wave, and the minus Mach line. Whilst conditions are fully known along this minus Mach line, these data are not sufficient to enable the mesh to be extended farther upstream since data along a plus Mach line also would be required.

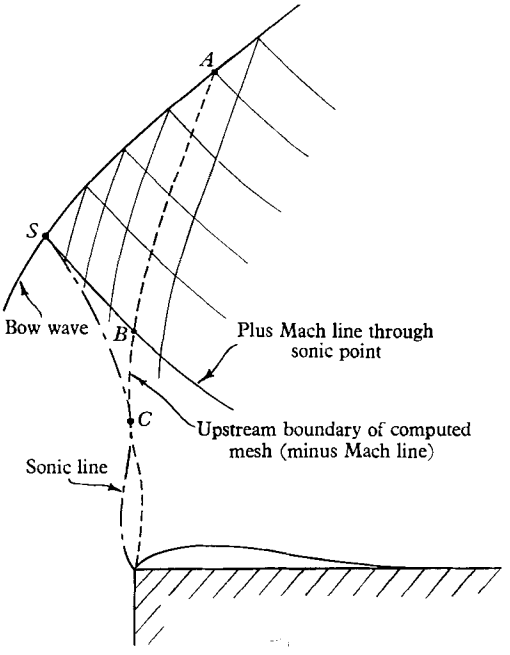

FIGURE 6. The indeterminate region.

Consideration has been given to the possibility of computing this zone by using base points on the bow wave outboard of the sonic point. This would not permit computation of the whole zone, but only that portion ABS which lies downstream of the plus Mach line through the sonic point. The undetermined portion of the sonic line, CS, would thus remain indeterminate by this method. It might, however, then be possible to use conditions along the present bounding minus Mach line, CA, and along the sonic point plus Mach line, SB, together. Whilst such a procedure seems feasible in principle, it would be inaccurate for the following reasons: (i) the present network and the bow wave are not in exact agreement at their intersection, A; (ii) the inevitable slight errors in t at the bow wave base points would be serious since in this region t is itself very small ($M \simeq 1$), but $\partial\mu/\partial t$ very large.

Under these circumstances, the scheme has not been pursued further.

The computed flow parameters at the network points have been used to draw in iso-Mach lines and streamlines by interpolation in μ and mass flow respectively. The network of Mach lines is shown in figures 7 and 8 and the resultant streamlines and iso-Mach lines in figure 9. These results will be discussed in § 5 below.

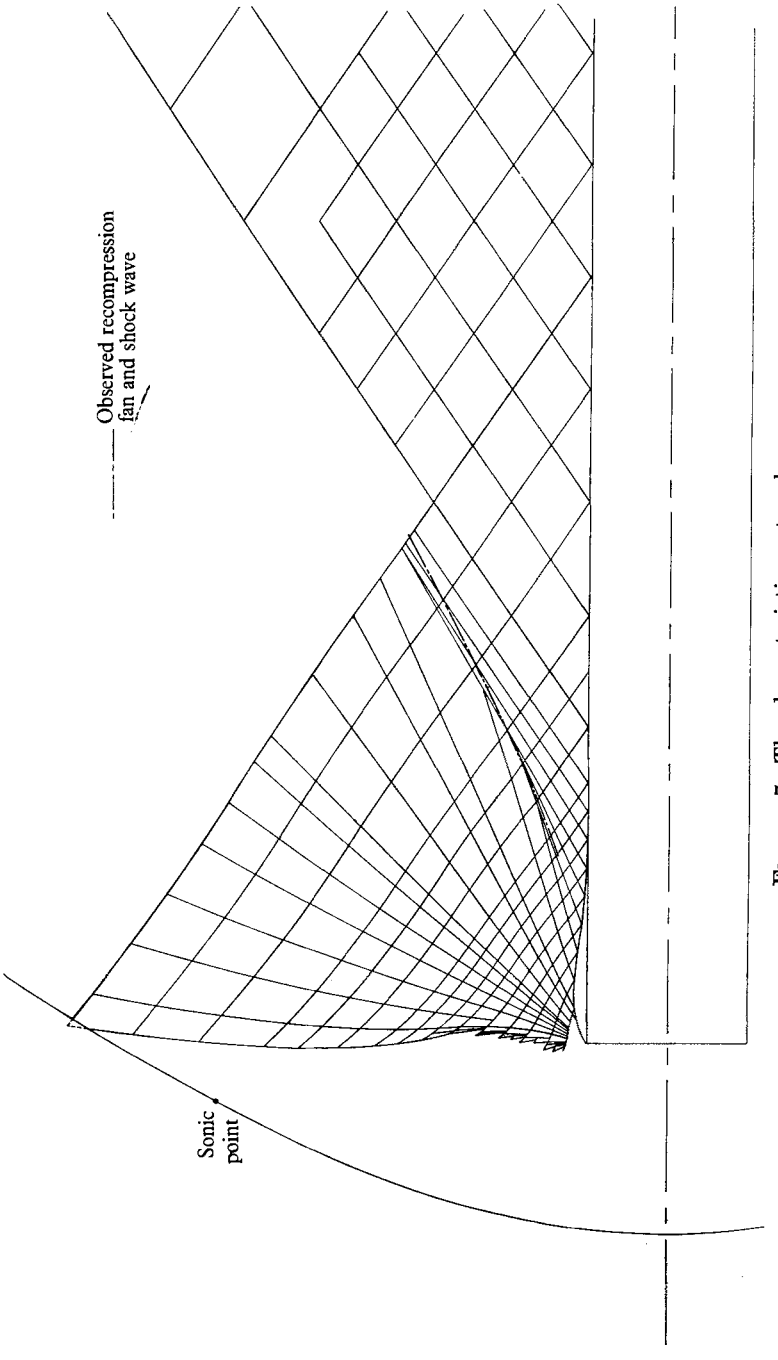

FIGURE 7. The characteristics network.

5. The computed flow field

5.1. *Conditions at the network-bow wave intersection*

It was of interest, when the characteristics network intersected the bow wave, to compare the network values of the flow parameters with those calculated from the shock wave equations at the relevant point. This is done in figure 10, where Mach number and flow direction downstream of a curved shock wave at $M = 1{\cdot}96$ are plotted against each other. Conditions at the intersection of the mesh and the bow wave, as predicted by the characteristics, are plotted as a single point for comparison.

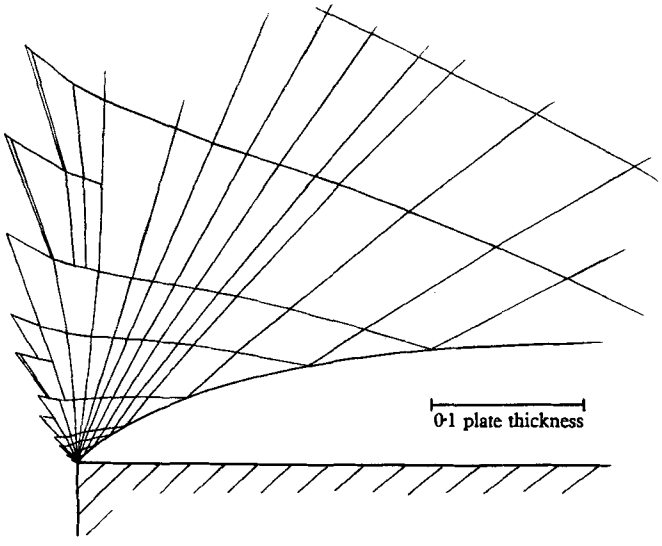

FIGURE 8. The nose region enlarged.

There are a number of sources from which the small discrepancy may arise: e.g. (i) errors in basic data, and incompatibility of curves fitted to boundary and bow wave; (ii) cumulative errors inevitable in any step-by-step method involving the use of mean quantities; (iii) neglect of the entropy change across the recompression shock may also have contributed.

Under these circumstances, the agreement is regarded as highly satisfactory, possibly due to the mutual cancellation of some errors.

It should be noted that the bow wave does not emerge from the computations as did the recompression shock wave. The bow wave results, as a normal shock wave, from the presence of a blunt-nosed body in the supersonic free stream. It thus enters the domain of the present calculations already determined, and is merely weakened by the incident expansion wavelets. As a result, the computation of the network did not in any way indicate the existence or location of the bow wave. Thus the mesh would have been extended farther outwards (into what is actually the free stream) had not photographic evidence of the bow wave location been available.

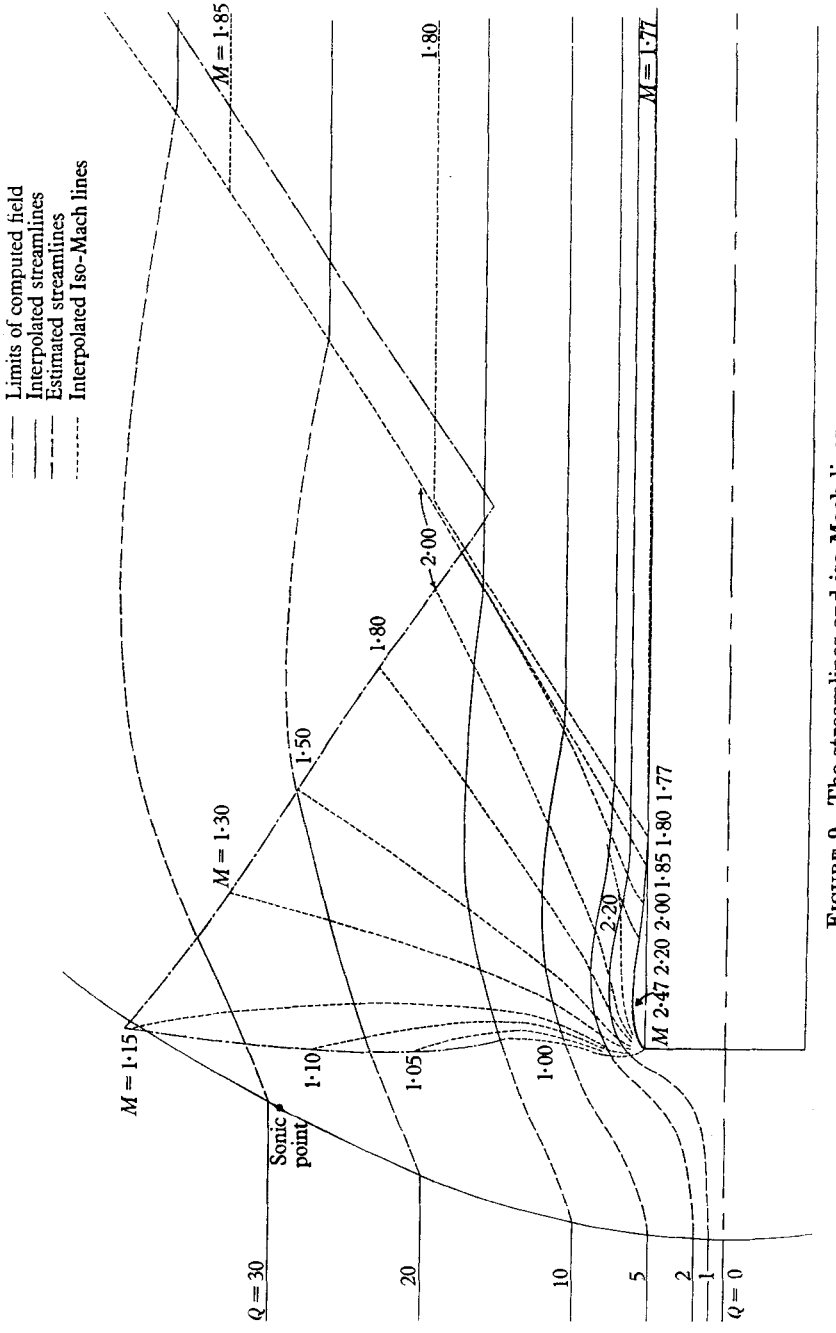

FIGURE 9. The streamlines and iso-Mach lines.

5.2. *The characteristics network (figures 7 and 8)*

The expansion Mach lines from the fan at the leading edge curve upstream and are reflected by the sonic line and bow wave back on to the surface as compression wavelets. Those which strike the sonic line form a cusp at that point, since the two Mach line families coincide at $M = 1{\cdot}00$. After a further reflexion from the surface, this time as compression waves, the Mach lines coalesce to form the recompression fan and shock wave, which agree well with the observed wave.

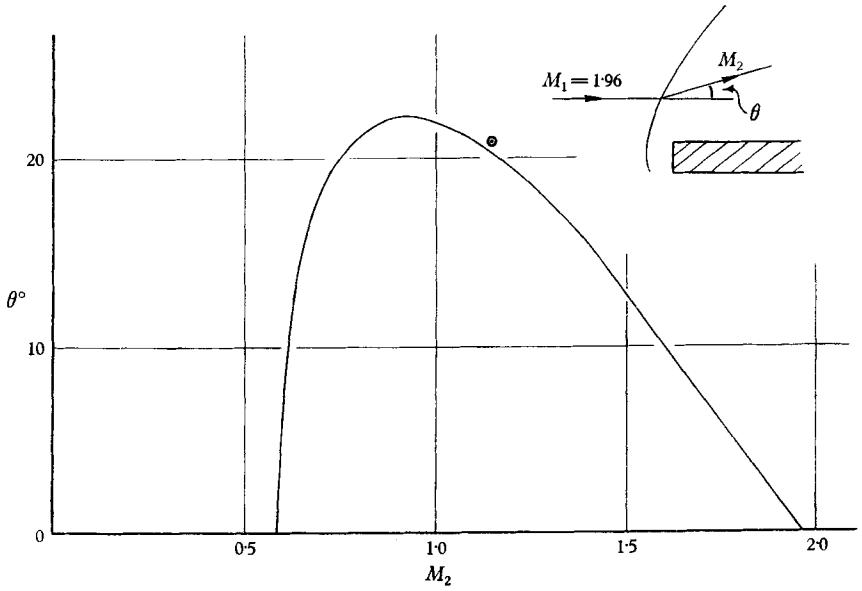

FIGURE 10. Accuracy of the characteristics network. ⊙ denotes computed values.

The leading expansion waves from the corner cause the sonic line to bulge upstream, and illustrate the manner in which it runs perpendicularly into the front face of the plate. The subsequent downstream bulge of the sonic line, followed by a further upstream bend, leads to the indeterminate region of supersonic flow ACS (see figure 6). In the first approximation, the sonic line would have become straight at C, approximately one plate thickness outboard of the surface, and would subsequently have coincided with a minus Mach line. The effect of the entropy correction has been to curve the sonic line upstream and the minus Mach line downstream, thereby producing between them the narrow triangular region, ACS, devoid of information along plus Mach lines. Accordingly, this triangular portion of the flow field cannot be computed by the present method. A possible alternative line of attack was considered in § 4.4 above, but was rejected for the reasons stated there.

Downstream of the recompression, the flow is parallel to the plate surface, but traversal of the curved bow wave has produced a gradient, normal to the surface, in entropy and hence in Mach number. The Mach lines in this region are slightly curved as a result.

5.3. *The streamlines and iso-Mach lines (figure 9)*

The streamlines have the expected shape; the subsonic portions have been drawn in qualitatively, but with the correct initial direction behind the bow wave. The entropy gradient referred to above leads to a gradient in mass flux. As a result, streamtubes of equal width in the free stream are no longer so downstream of the recompression. The displacement effect of the plate on the streamlines falls off with perpendicular distance from the plate.

The expansion fan from the leading edge accelerates the flow from $M = 1$ to $M = 2{\cdot}47$. The latter Mach number, the highest attained throughout the flow field, corresponds to the constant pressure portion of the separation bubble from the leading edge to just beyond the point of maximum height. This part of the bubble profile is thus the iso-Mach line of $M = 2{\cdot}47$.

The iso-Mach lines may be divided into two types:

(i) $M > M_1$ (where M_1 is free stream Mach number). These form closed curves; commencing in the expansion fan, they curve outwards and downstream, form a cusp in the recompression shock, and then descend again to the surface via the recompression fan. They thus enclose embedded regions of Mach number greater than their own, e.g. $M = 2{\cdot}0, 2{\cdot}2$ in figure 8. The case of $M = 2{\cdot}47$ discussed above is the limiting case of this type, in which the embedded region has collapsed on to the bubble profile.

(ii) $M < M_1$. These also commence in the leading edge fan, curve downstream, and then upstream again. They thus intersect the bow wave and not the recompression shock. For $M \geqslant 1{\cdot}77$, they possess another branch which rises from the concave portion of the bubble surface, through the recompression fan, and then turns downstream, parallel to the surface and coinciding with a streamline, e.g. $M = 1{\cdot}80$. $M = 1{\cdot}77$ is the limiting case of this type, being the constant Mach number along the plate surface downstream of the recompression region.

The iso-Mach line of $M = 2{\cdot}47$ has the same shape as the bubble profile since it coincides with that profile. It will also be noted that the remainder of the iso-Mach lines from the leading edge have this shape, which appears to be transmitted up the plus Mach lines. The similarity was heightened when the entropy correction was omitted, since the iso-Mach lines eventually became straight, corresponding to the flat surface downstream of the bubble reattachment point. The entropy correction subsequently produced the gentle upstream curvature in this region.

The shape of the outer portion of the sonic line, not calculable by the present technique, may be inferred from that of the $M = 1{\cdot}15$ iso-Mach line. In view of the slight discrepancy noted between the bow wave and the characteristics mesh, it is unlikely that the computed sonic line would pass through the bow wave sonic point marked. It would probably intersect the bow wave some distance inboard of this point.

The pattern of iso-Mach lines forms an interesting comparison and contrast with figure 11 of the paper by Roy (1957) which is reproduced here as figure 11. This figure, obtained from an interferogram, shows the streamlines and iso-Mach lines in the flow past a plate with a rounded leading edge. The Mach number was identical with that of the present work, namely 1·96. It is therefore instructive

to compare the two patterns, one taken from experimental observation, the other also derived from experimental data, but after lengthy step-by-step computations.

The different leading edge configuration has a considerable effect, of course, in that the rounded leading edge eliminates the separation bubble and subsequent recompression. Far downstream of the leading edge, however, agreement would be expected, and the streamlines and iso-Mach lines in this region do compare well, e.g. $M = 1{\cdot}80$. The absence of the bubble removes the distortion from the inboard ends of the leading edge iso-Mach lines, which therefore curve smoothly outwards to the bow wave. Again, since there is no bubble to accelerate the flow beyond the free stream Mach number, there is no embedded pocket of such flow, and a recompression shock wave is unnecessary.

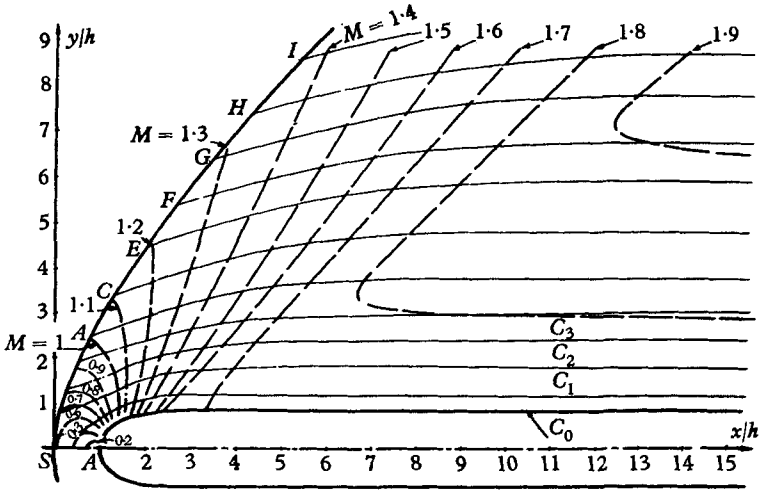

FIGURE 11. Flow past a plate with a rounded leading edge; reproduced from Roy (1957).

6. Conclusions

Commencing from the experimental observations of the flow direction and Mach number along the surface of the square-nosed flat plate with separation bubble at $M = 1{\cdot}96$, the external supersonic flow field has been computed by the method of characteristics. It has proved feasible to work upstream and outwards from the surface, as far as the sonic line and bow wave. The entropy gradient due to the curved bow wave has been incorporated in the calculations, and a special technique has been used for the region close to the sonic line. A small portion of the flow field, including the outer end of the sonic line has proved to be indeterminate by this method.

The values of the flow parameters at the mesh points have been used to plot streamlines and iso-Mach lines by interpolation. The agreement between the flow parameters predicted by the characteristics and by the shock wave equations at the network–bow wave intersection was found to be excellent. The iso-Mach line pattern has afforded an interesting comparison with results obtained in France by interferometry for a differently shaped leading edge at the same Mach number.

The author is particularly indebted to Dr N. H. Johannesen and to Prof. P. R. Owen for suggestions and advice during the course of the work, and to the Department of Scientific and Industrial Research for a maintenance grant. Thanks are due to M. Maurice Roy, Directeur-Général de l'O.N.E.R.A., for permission to reproduce figure 11.

REFERENCES

BARDSLEY, O. & MAIR, W. A. 1951 *Phil. Mag.* **42**, 29.

HERBERT, P. J. & OLDER, S. J. 1946 *Roy. Aircr. Estab., Tech. Note* no. C.W. 1.

HOLDER, D. W. & CHINNECK, A. 1954 *Aero. Quart.* **4**, 317.

HOLT, M. 1949 *Quart. J. Mech. Appl. Math.* **2**, 246.

MEYER, R. E. 1948 *Quart. J. Mech. Appl. Math.* **1**, 196.

ROY, M. 1957 *O.N.E.R.A.*, Publ. no. 90. (Further details are given in *La Rech. Aero.* no. 60, 1957.)